

NOTE

A black-blood ultra-short echo time (UTE) sequence for 3D isotropic resolution imaging of the lungs

Jean Delacoste¹  | Helene Feliciano¹ | Jérôme Yerly^{1,2} | Vincent Dunet¹ | Catherine Beigelman-Aubry¹ | Giulia Ginami^{1,3}  | Ruud B. van Heeswijk^{1,2}  | Davide Piccini^{1,4} | Matthias Stuber^{1,2} | Alain Sauty^{5,6}

¹Department of Radiology, University Hospital (CHUV) and University of Lausanne (UNIL), Lausanne, Switzerland

²Center for Biomedical Imaging (CIBM), Lausanne, Switzerland

³School of Biomedical Engineering and Imaging Sciences, King's College London, London, United Kingdom

⁴Advanced Clinical Imaging Technology, Siemens Healthcare AG, Lausanne, Switzerland

⁵Adult CF unit, Neuchâtelois-Pourtales Hospital, Neuchâtel, Switzerland

⁶Service of Pneumology, Department of Medicine, University Hospital (CHUV), Lausanne, Switzerland

Correspondence

Alain Sauty, Hôpital Neuchâtelois-Pourtales, Département de médecine, Maladière 45, 2000 Neuchâtel, Switzerland.
Email: asauty@gmail.com

Funding information

This work is supported by a grant from the Fondation BCV and by Swiss National Science Foundation grant 320030_143923.

Purpose: Ultra-short echo time MRI is a promising alternative to chest CT for cystic fibrosis patients. Black-blood imaging in particular could help discern small-sized anomalies, such as mucoid plugging, which may otherwise be confused with neighboring blood vessels, particularly when contrast agent is not used. We, therefore, implemented and tested an ultra-short echo time sequence with black-blood preparation. Additionally, this sequence may also be used to generate bright-blood angiograms.

Methods: Using this sequence, data was acquired during free breathing in 10 healthy volunteers to obtain respiratory-motion-resolved 3D volumes covering the entire thorax with an isotropic resolution of (1 mm)³. The magnitude of signal suppression relative to a bright-blood reference acquisition was quantified and compared with that obtained with a turbo-spin echo (TSE) acquisition. Bright-blood angiograms were also generated by subtraction. Finally, an initial feasibility assessment was performed in 2 cystic fibrosis patients, and images were visually compared with contrast-enhanced images and with CT data.

Results: Black-blood preparation significantly decreased the average normalized signal intensity in the vessel lumen (−66%; $P < 0.001$). Similarly, blood signal was significantly lowered (−60%; $P = 0.001$) compared with the TSE acquisition. In patients, mucoid plugging could be emphasized in the black-blood datasets. An intercostal artery could also be visualized in the subtraction angiograms.

Conclusion: Black-blood free-breathing ultra-short echo time imaging was successfully implemented and motion-resolved full volumetric coverage of the lungs with high spatial resolution was achieved, while obtaining an angiogram without contrast agent injection. Encouraging initial results in patients prompt further investigations in a larger cohort.

KEYWORDS

black-blood, MSDE, UTE

1 | INTRODUCTION

MRI has gained growing interest as an alternative to CT for the assessment of lung disease.¹ The absence of ionizing radiation is particularly advantageous in the context of chronic diseases that require repeated imaging studies as, for example, cystic fibrosis (CF).^{2,3} Lung MRI is challenging due to multiple potential sources of artifacts, such as organ motion and the very short T_2^* of the lung parenchyma (2 ms at 1.5T).⁴ While imaging at 3T field strength can result in higher signal-to-noise ratio, the T_2^* is also further shortened to approximately 0.5 ms, which renders lung imaging at 3T particularly challenging.⁴ Due to their capacity to image short T_2^* components, ultra-short echo time (UTE) sequences^{5,6} have been developed for lung imaging and their usefulness in the assessment of CF has been demonstrated.⁷⁻¹⁰

CF patients typically present with bronchorrhea (large production of sputum), which is associated with diffuse bronchial dilations predominantly located in the upper lobes. Airways filled with mucoid secretions, referred to as mucoid plugging, may be hard to differentiate from blood vessels in certain cases,¹¹ especially when bronchial structures cannot be clearly distinguished due to limited spatial resolution. Although technical advances allow finer spatial resolutions to be achieved with MRI, some morphological features may still be difficult to visualize, particularly at distal levels of bronchial and pulmonary artery divisions. Contrast agent injection can help distinguish mucoid impactions, that do not show enhancement, from bronchial wall thickening and arteries, that do.^{2,12,13}

In cases where contrast agent injection is not carried out, blood signal suppression^{14,15} could potentially provide an alternative to help distinguish, e.g., fluid in small airways (mucoid plugging) from blood in the neighboring arteries, as the interface separating these 2 anatomical structures may not be directly observed due to their small calibers and taking into account their similar direction. Also, in the lung periphery, small airways disease commonly presents as tree in bud pattern^{12,13} that may be underestimated due to a lack of spatial resolution, which reinforces the interest of complementary methods.

CF may also cause changes in lung vasculature. Hemoptysis (i.e., coughing up of blood) is a serious life-threatening complication of the disease.¹⁶ It is caused by chronic inflammation in the lungs, which leads to hypertrophy of the bronchial arteries that increases the risk of hemorrhage.¹⁶ Bleeding

may also occur from nonbronchial systemic collateral vessels.^{16,17} These vessels may originate from various arteries, such as intercostal arteries, branches of the subclavian or axillary arteries or inferior phrenic arteries.¹⁸ Hypertrophied bronchial and nonbronchial systemic arteries can be observed with CT angiography.^{18,19} Although these vessels may be studied without exposure to ionizing radiation by using MRI with contrast agent injection,^{12,20} a method allowing the visualization of these vessels without requiring contrast agent injection may provide a valuable alternative.

Motion-sensitized driven equilibrium (MSDE) preparation was originally introduced for liver imaging to suppress bright signals, notably from vessels, that could otherwise be confused with high intensity lesions.²¹ The main goal of the present work was to implement the combination of MSDE preparation with a previously described free-breathing self-navigated UTE sequence⁸ to produce high resolution 3D black-blood images of the lung.²² In particular, the hypothesis was that blood signal could be more efficiently suppressed with this method than with a turbo-spin echo sequence acquired in breath-hold.

Related to the issue of hemoptysis, a second goal of this study was to investigate the use of a bright-blood UTE acquisition in conjunction with the black-blood sequence mentioned above to create an angiogram of the thoracic vessels, using a method similar to the one introduced by Fan et al²³ for imaging of the lower extremities. In this context of MR angiography, an added advantage of UTE sequences is their increased robustness against flow dephasing.^{24,25}

2 | METHODS

An MSDE blood signal suppression module^{21,26} was implemented and added to a prototype 3D UTE sequence (Figure 1). The UTE acquisition was performed with a segmented 3D radial spiral phyllotaxis trajectory,²⁷ which enables respiratory motion detection²⁸ for retrospective gating.⁸ This pulse sequence was tested in ten healthy volunteers and preliminarily compared with the gold standard CT for 2 CF patients.

2.1 | Blood signal suppression

The MSDE module was implemented by modifying an existing²⁹ adiabatic T_2 preparation module, consisting of a 90°

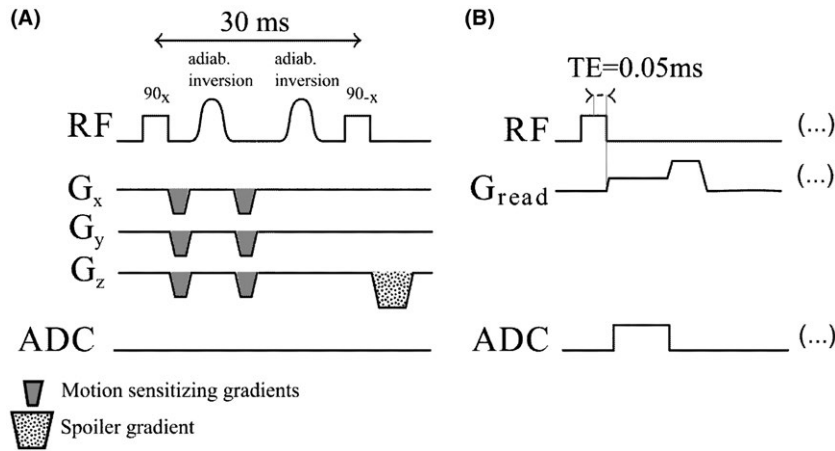


FIGURE 1 Schematic overview of the pulse sequence. The MSDE module (A) is a modified adiabatic T_2 preparation module where additional gradient moments result in dephasing of spins moving in any direction. The module is followed by a train of UTE readouts (B)

rectangular excitation pulse, followed by 2 adiabatic hyperbolic secant inversion pulses and a final rectangular -90° restoring pulse.³⁰⁻³² To achieve motion sensitization, a trapezoidal gradient is applied along the 3 major gradient axes²⁶ between the 90° excitation pulse and first inversion pulse. A second gradient of identical moment to the first one is then played out after the first inversion pulse. Thus the phase of the magnetization of static spins is restored while flowing spins will keep a phase offset.

Depending on the offset, the magnetization of these flowing spins will not be restored to the longitudinal axis by the final -90° pulse and, therefore, will be spoiled by the final gradient of the module before the imaging sequence is run. The efficiency of signal suppression depends on the gradient moments used within the MSDE module and the speed of flowing spins. Based on the gradient moment used and the delay between the 2 lobes, the field of speed (FOS) can be calculated, which indicates the velocities for which a phase shift of 2π will be induced.³³

2.2 | Respiratory motion suppression

The segmented 3D radial spiral phyllotaxis trajectory of the UTE sequence used in this work acquires a projection of the image volume in the superior-inferior direction at the beginning of each interleaf, which can be used for respiratory self-navigation.²⁸ Conventionally, the blood pool is automatically segmented in these projections based on the contrast with the surrounding structures.^{8,28} However, because blood signal is suppressed by the MSDE preparation module, motion suppression methods relying on the contrast between the blood pool and surrounding tissue are impractical. Therefore, in this study, a previously reported iterative algorithm³⁴ that does not rely on blood pool segmentation was used to detect the vertical component of respiratory motion across superior-inferior projections.

2.3 | Healthy volunteer study

2.3.1 | Data acquisition and image reconstruction

High resolution (1 mm isotropic) datasets were acquired in 10 healthy volunteers using a 3T clinical MRI scanner (MAGNETOM Prisma, Siemens Healthcare, Erlangen, Germany). All volunteers provided written informed consent in this ethics committee approved study. The total acquisition duration was recorded. Acquisition parameters were: echo time (TE) = 0.05 ms, pulse repetition time (TR) = 5.6 ms, readout bandwidth = 399 Hz/px, radiofrequency excitation angle = 5° , field of view = $(250 \text{ mm})^3$, number of k-space samples per radial readout = 256 (2-fold oversampling), reconstruction matrix size = 256^3 , voxel resolution = $(1 \text{ mm})^3$ and 398 segments consisting each of 44 readouts. Electrocardiogram triggering was used to acquire segments every other heart beat in diastole to allow time for magnetization recovery. For each volunteer, 2 acquisitions were performed with black-blood preparation enabled, using FOS values of 10 and 20 cm/s as the independent variable. This range of values was similar to that used in other studies of MSDE preparation.³³ The 10 cm/s value was the lowest value achievable with this implementation without reaching the threshold for peripheral nerve stimulation. Additionally, a reference dataset was obtained with identical sequence parameters except that the MSDE module was played out without any motion sensitizing gradients.

To achieve motion suppression, 4 respiratory frames were reconstructed for each acquisition. To this end, the respiratory signal was used to separate the data in 4 bins, containing 25% of the data each, which resulted in further undersampling. Therefore, motion-resolved datasets were reconstructed using a compressed sensing algorithm exploiting sparsity in both the spatial and respiratory dimensions^{35,36} with the following model³⁷:

$$\hat{\mathbf{d}} = \arg \min_{\mathbf{d}} \|\mathbf{F} \cdot \mathbf{C} \cdot \mathbf{d} - \mathbf{m}\|_2^2 + \lambda_1 \|\boldsymbol{\psi} \cdot \mathbf{d}\|_1 + \lambda_2 \|\nabla_{\text{spat}} \cdot \mathbf{d}\|_1 + \lambda_3 \|\nabla_{\text{resp}} \cdot \mathbf{d}\|_1$$

where $\hat{\mathbf{d}}$ is the final image reconstructed, which provides an optimized solution minimizing the right hand side of the equation. \mathbf{d} is an image variable, \mathbf{F} is the nonuniform fast Fourier transform operator from image space to k-space, \mathbf{C} is the coil sensitivity matrix, \mathbf{m} is the k-space raw data, $\boldsymbol{\psi}$ is a spatial wavelet transform, ∇_{spat} is a first order finite differences operator in the spatial dimension, and ∇_{resp} is a first order finite differences operator along the respiratory dimension. The regularization parameters λ_{1-3} were optimized empirically and the same values ($\lambda_1 = 0.005$, $\lambda_2 = 0.005$, $\lambda_3 = 0.05$) were used for all reconstructions. After image reconstruction, angiograms were also generated by subtracting the motion-sensitized datasets from the reference datasets (magnitude images).²³ As a reference for sharpness measurements, motion corrupted datasets were also reconstructed with standard nonuniform Fourier transform.

UTE datasets were compared with a turbo-spin echo sequence with rotating phase encoding (BLADE),³⁸ as such sequences are clinically indicated for imaging of the lungs,^{39,40} and usually acquired in multiple breath-holds.¹ Slices were acquired in a coronal orientation with the following parameters: TE = 89 ms, TR = 2020 ms, echo spacing = 5.59 ms, echo train length = 31, field of view = (400 mm)², pixel resolution = (1.25 mm)², 39 slices, echo trains per slice = 10, slice thickness = 3 mm, generalized autocalibrating partial parallel acquisition (GRAPPA) acceleration factor = 2. The acquisition was segmented in 6 consecutive breath-holds of 20 s each.

2.3.2 | Data analysis

The magnitude of blood signal suppression was quantified by measuring the normalized signal intensity in the vessel lumen in 4 locations in the datasets: the right and left pulmonary artery and the ascending and descending aorta. The normalized signal intensity was defined as the mean signal intensity in a region of interest (ROI) manually drawn on the vessel lumen divided by the mean signal intensity in a ROI drawn in the air outside of the chest wall. As the dependent variable, the average normalized signal intensity over all locations was compared for the 3 acquisition parameters. In addition, the standard deviation across the 4 ROI was computed for each volunteer to obtain a measure of the interluminal variability. Statistical significance was assessed using a paired Student's t-test with Holm's correction for multiple comparisons.⁴¹ P values lower than 0.05 were considered statistically significant.

Signal suppression was also quantified visually as follows: The reference image and the FOS = 10 cm/s images

were displayed side-by-side on a viewing console. Two experts in chest imaging (C.B.A. and V.D.) scored the efficiency of signal suppression in consensus at the lobar, segmental, sub-segmental, and below sub-segmental level until the periphery in each lobe. Possible score values were 4 = 75-100% of signal suppressed, 3 = 50-75% of signal suppressed, 2 = 25-50% of signal suppressed, 1 = 0-25% of signal suppressed. A Wilcoxon signed rank test with Holm's correction was used to assess statistical significance.

To assess the performance of the motion suppression technique, the sharpness of the transition at the lung-liver interface was quantified by computing the normalized maximum of the first derivative (MD)⁴² on the 4 reconstructed respiratory frames. The maximum of the first derivative was computed along 21 vertical profiles going through the lung-liver interface and the value measured in each profile was normalized to the value measured in the corresponding profiles of the motion corrupted datasets. With this definition, a value larger than 1.0 indicates a sharpness increase, while values smaller than 1.0 indicate decreased image definition. The significance of the difference with respect to 1.0 was assessed for each frame with a 1-sample t-test. P values lower than 0.05 were considered statistically significant.

2.4 | Feasibility in CF patients

A preliminary assessment of the potential of this method was performed in 2 adult CF patients with genetically and clinically confirmed diagnosis. All participants provided written informed consent in this ethics committee approved study.

Acquisition and reconstruction parameters were the same as those used in the volunteer study. However, to accommodate time constraints, only a single dataset with a FOS value of 10 cm/s was acquired in patient 1, while 2 datasets could be acquired in patient 2 (reference and FOS = 10 cm/s).

The datasets were qualitatively assessed in terms of blood signal suppression, vessel depiction, and visibility of mucoid plugging and bronchiectasis. Additionally, images were compared with those obtained with the most recent clinically indicated CT and to contrast-enhanced images obtained with a 3D spoiled gradient echo sequence (Volumetric Interpolated Breath-hold Examination, VIBE, Siemens) on the same day using a 1.5T clinical scanner (MAGNETOM Aera, Siemens Healthcare, Erlangen, Germany). Acquisition parameters were: TE₁ = 2.99, TE₂ = 4.77, TR = 6.76, readout bandwidth = 475 Hz/px, radiofrequency excitation angle = 10°, field of view = (250 mm)³, matrix size = 320 × 218, reconstructed image size = 320 × 290, 120 slices, pixel resolution = (1.18 mm)²,

slice thickness = 1.5 mm. Images were reconstructed using Dixon's method for water-fat separation.⁴³

3 | RESULTS

3.1 | Healthy volunteer study

Data acquisition was 15 ± 2 min long on average for each UTE dataset. The normalized signal intensity in the vessel lumen, averaged over the 4 ROI locations, was significantly lower with both FOS values when compared with the reference datasets (Figure 2A, FOS = 10 cm/s: $P = 0.001$, FOS = 20 cm/s: $P < 0.001$). When compared with the BLADE acquisition, the use of UTE with MSDE preparation also resulted in significantly lower signal intensity in the lumen of the vessels studied with both FOS values (FOS = 10 cm/s: $P = 0.001$, FOS = 20 cm/s: $P < 0.001$). However, no significant difference between these 2 FOS values was measured.

Suppression of blood signal could be observed in all vessels, despite different spatial orientations (Figure 3A-C). The interluminal variability (Figure 2B) was also significantly lower when MSDE UTE was used compared with the reference acquisition (FOS = 10 cm/s: $P < 0.001$, FOS = 20 cm/s: $P < 0.001$) and BLADE acquisition (FOS = 10 cm/s: $P < 0.001$, FOS = 20 cm/s: $P < 0.001$). Indeed, more homogeneous blood signal suppression was observed when using MSDE UTE compared with BLADE, as seen in Figure 3D,G. Misregistration artifacts due to imperfect lung volume reproduction at each breath-hold were often observed in images acquired with the BLADE sequence (e.g., Figure 3H) but not when MSDE UTE was used (e.g., Figure 3E).

Visual evaluation of signal suppression in FOS = 10 cm/s images (Figure 2C) indicated very high signal suppression at the lobar and segmental arterial levels (median score = 4, indicating 75-100% signal suppressed). The efficiency of signal suppression decreased gradually for the sub-segmental

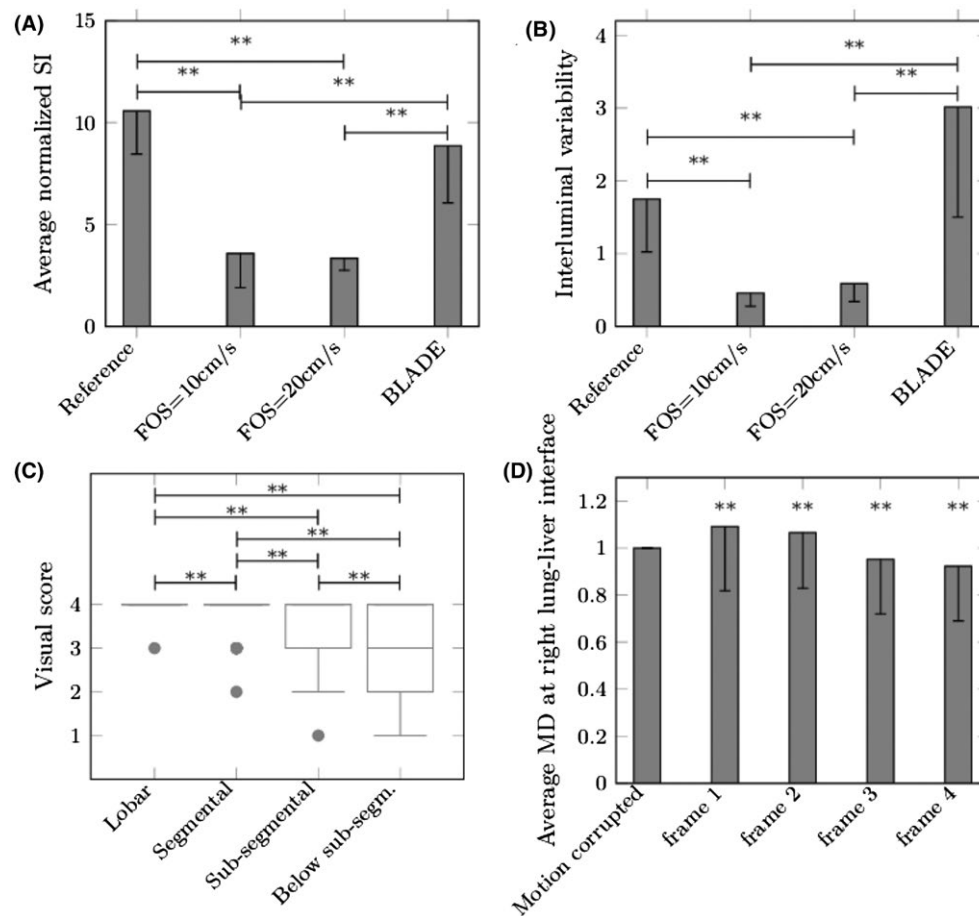


FIGURE 2 The average normalized signal intensity (SI) over all volunteers (A) was significantly lower in the black-blood prepared images than in the reference datasets. UTE MSDE resulted in lower residual signal intensity in the lumen than when a BLADE acquisition was used. FOS values of 10 and 20 cm/s had significantly lower variability (B) between residual luminal signal than the reference and BLADE datasets. Visual scoring of signal suppression (FOS = 10 cm/s compared with reference) in pulmonary arteries (C) showed slightly decreasing efficiency of signal suppression at sub-segmental level and below. The normalized maximum of the first derivative (D) was significantly larger than 1.0 in frames 1 and 2 (expiratory datasets) and significantly lower than 1.0 in frames 3 and 4 (inspiratory datasets). $**P < 0.01$

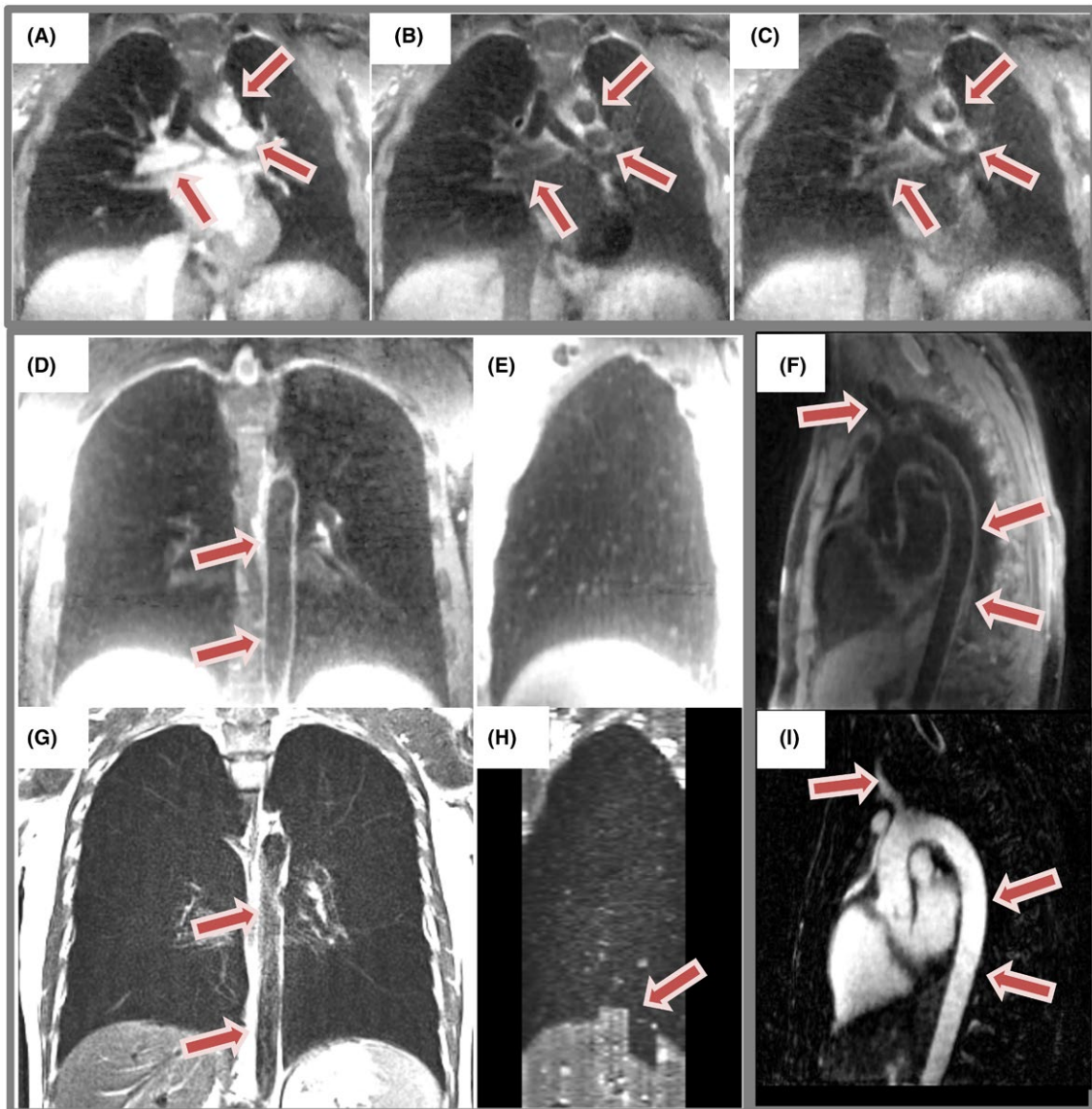


FIGURE 3 Example coronal reformats from volunteer 1. Compared with the reference image (A), blood signal is well suppressed in the black-blood images (B: FOS = 10 cm/s, C: FOS = 20 cm/s) in the aortic arch and left and right branches of the pulmonary artery (arrows) despite different spatial orientations of these vessels. Coronal reformats of frame 1 of a black-blood UTE image acquired with FOS = 10 cm/s in volunteer 7 (D) show more homogeneous signal suppression in aorta (arrows) than with BLADE acquisition (G). Sagittal reformat of black-blood UTE image shows isotropic resolution and artifact free depiction of the liver dome (E), while in anisotropic BLADE image (H), the liver dome is improperly depicted because of inadequate breath-hold reproduction (arrow). Multiplanar reformat of data acquired in volunteer 5 shows blood signal suppression in the FOS = 10 cm/s black-blood UTE image (F) in the aorta and right common carotid artery. The aortic wall can be well identified over its entire length. In the subtraction image (I), the signal from vessels is enhanced with respect to other tissues while no contrast agent was needed

level and below (median score = 3, indicating 50-75% signal suppression).

The diaphragm definition, quantified with MD (Figure 2D) was significantly improved in expiratory respiratory frames (frames 1 and 2; $P < 0.001$) when compared with the motion corrupted acquisition. Conversely, significantly decreased diaphragmatic sharpness was measured in inspiratory datasets (frames 3 and 4; $P < 0.001$).

Thoracic vessels could be visualized with the proposed technique, as can be seen for example in the aorta of volunteer 5 (Figure 3F). Angiograms, obtained by subtraction, yielded a bright signal from all flowing structures in the FOV, regardless of their spatial orientation or flow velocity. Notably, blood signal was enhanced, which allowed visualization of the vessels without requiring contrast injection (Figure 3I).

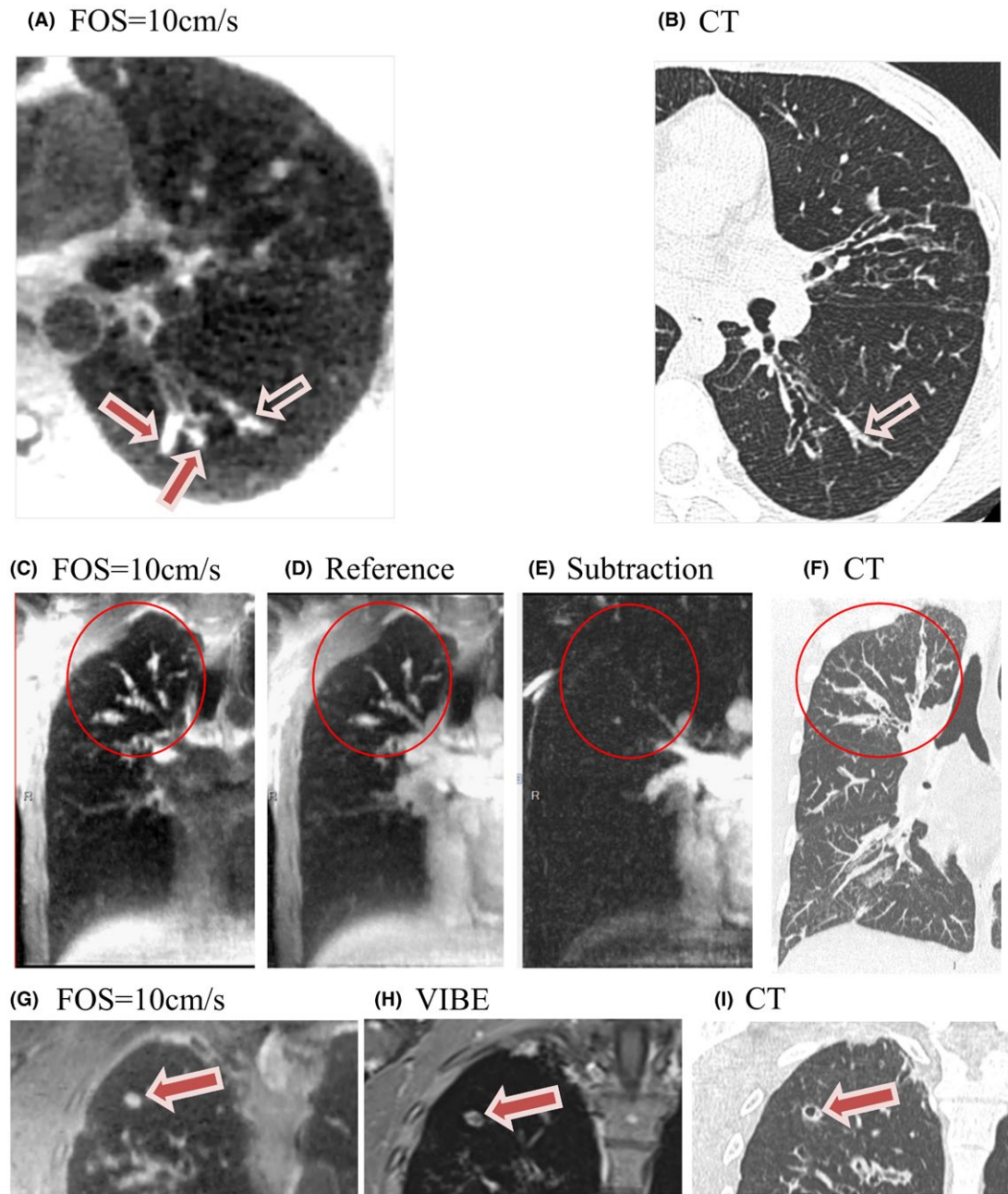


FIGURE 4 In patient 2, the black-blood UTE image (A) shows several mucoid impactions within bronchiectasis, distal to the sub-subsegmental level of the apical segment of the left lower lobe (arrows), that subsequently partially disappeared with persistence of the most lateral of them (hollow arrow) on the equivalent CT image (B) acquired 3 days later. Tubular structures with bright signal on 4-mm-thick maximum intensity projections of black-blood (C) and bright-blood (D) images, corresponding to mucoid impactions within bronchiectasis of the right upper lobe, are suppressed in the subtraction image (E). Note that these structures perfectly match with the CT findings (F). A mucoid impaction in the upper right lobe, viewed on a black-blood UTE image (G) can also be seen on a contrast-enhanced acquisition (H) where, additionally, the airway boundary can be observed. The impaction disappeared on the CT image (I) acquired 3 days later

3.2 | Feasibility in CF patients

Blood signal appeared well suppressed in the CF patients and mucoid impactions exhibited high signal in the black-blood images (Figure 4A,C,G). These findings were matched to the equivalent CT data (Figure 4B,F,I) taking into account that

some impactions disappeared during the 3-day period separating MRI from the CT examination. Signal from mucoid impactions was cancelled on subtraction images (Figure 4E). Mucoid impactions could also be observed on contrast-enhanced gradient echo images and clearly differentiated from the enhanced bronchial parietal walls (Figure 4H).

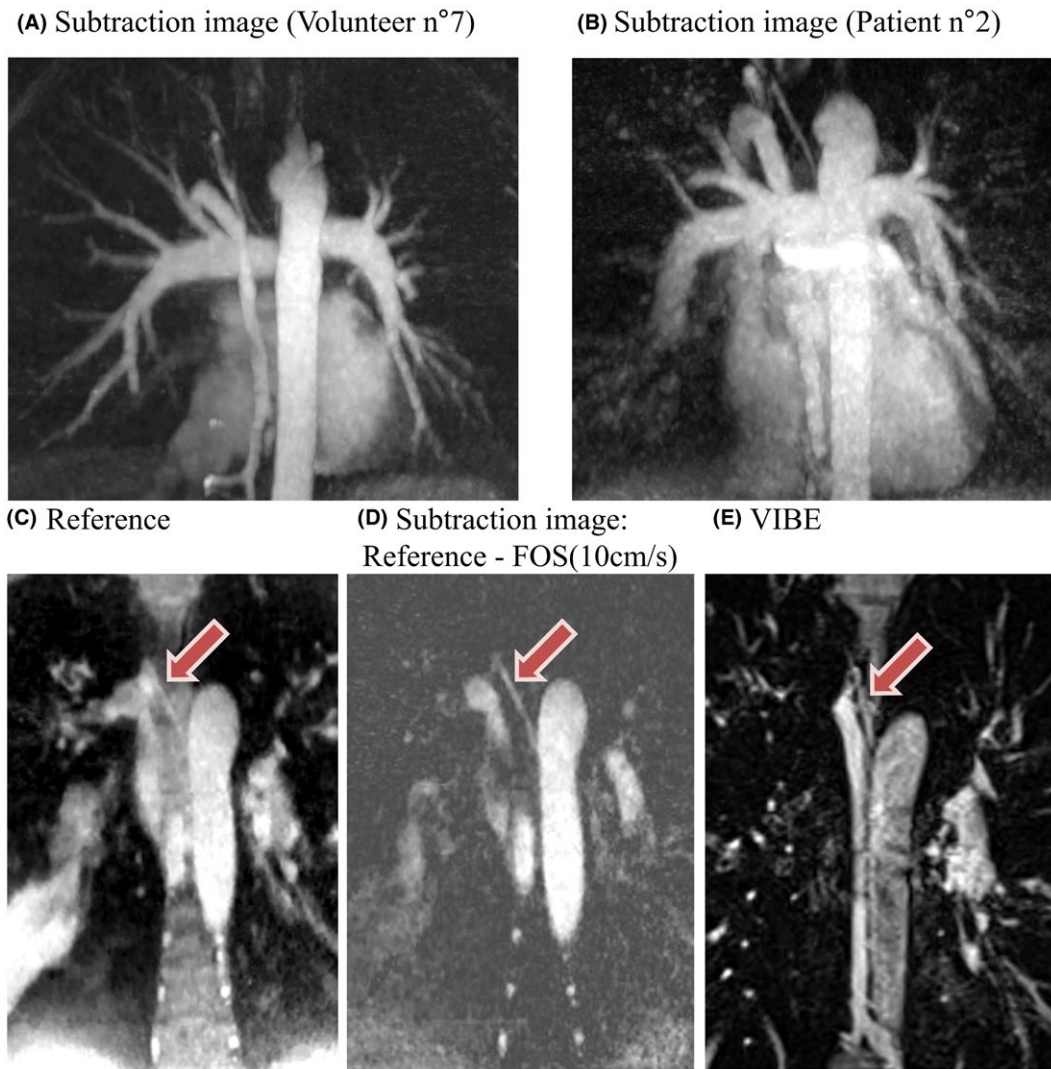


FIGURE 5 No subtraction artifacts were visible on MR subtraction angiography (40mm-thick maximum intensity projection coronal image) showing pulmonary arteries in volunteer 7 (A). Comparable image quality was achieved in patient 2 (B). At the time of the MR exam, bronchopneumonia involving the lower lobes may have altered the visualization of the lower pulmonary arteries. For the same patient, a right intercostal artery can be distinguished in a coronal reformat of the reference bright-blood UTE image (C). Visualization of this artery is simplified in the subtraction angiography image (D), as signal from stationary structures is cancelled. This artery may also be viewed on a contrast-enhanced acquisition (E), although the origin of the vessel may not be observed

The main thoracic vessels were well depicted in the subtraction dataset (Figure 5B) with comparable image quality to that achieved in healthy volunteers (Figure 5A). Smaller caliber vessels such as an intercostal artery could also be visualized in subtraction images (Figure 5D), with more ease than on bright-blood images (Figure 5C), and matched with observations on contrast-enhanced gradient echo acquisition (Figure 5E).

4 | DISCUSSION AND CONCLUSION

High resolution 3D isotropic black-blood UTE imaging was enabled with the proposed technique, and the results

confirmed the significant decrease in signal from the arterial lumen. Significantly better results were obtained with the MSDE UTE method than with the compared BLADE acquisition. Visual evaluation of the FOS = 10 cm/s confirmed blood-signal suppression in pulmonary arteries, albeit with decreasing efficiency when exploring lower subdivision levels. While no significant differences in ROI statistics could be seen between the 2 FOS values used in the study, lower FOS values intuitively seem preferable as they should improve suppression of signal from slower flow, such as in the distal arteries and veins. These considerations guided the choice of the 10 cm/s FOS value for the initial test in patients.

Notwithstanding the good results obtained with a FOS value of 10 cm/s, extended studies in a larger cohort, therefore, remain necessary to further explore the range of optimal

FOS values and to determine what value suppresses the most blood-signal without suppressing signal from slow moving tissues. However, modifications to the MSDE preparation implementation are necessary to explore lower FOS values than those tested in this study. In this study, the MSDE preparation was applied during diastole. As arterial flow should be higher than in the diastolic period, further investigations should study whether shifting the preparation to the systolic period could provide better blood-signal suppression. This may, however, also result in suppression of signal in moving tissue close to the heart.

Another area requiring further investigation is the spatial orientation of the motion sensitizing gradients, as in this study identical moments were applied along each gradient axis. Individual optimization of the gradient strength for each physical direction could potentially improve signal suppression.

Blood signal was significantly more suppressed when using MSDE UTE than with the turbo-spin echo sequence used as comparison (BLADE). Additionally, as the BLADE sequence was acquired in multiple breath-holds, misregistration artifacts between acquired slabs affected image quality. Inhomogeneous signal suppression was also observed in BLADE images (e.g., Figures 2B and 3G), most likely due to in plane flow, which results in loss of dark-blood contrast.⁴⁴ These effects were not observed when acquiring with MSDE UTE. However, MSDE UTE images present higher apparent noise level, which may be related to the 3D radial nature of the acquisition. Nevertheless, the isotropic resolution of the UTE sequence allowed reformation in any direction, which could facilitate clinical use and provide an advantage compared with the BLADE sequence.

The requirement to acquire data every other heart beat results in prolonged acquisition time for the UTE MSDE sequence (15 min). However, interlacing bright-blood and black-blood acquisitions could potentially increase scan efficiency. The incorporation of the signal model in the compressed sensing reconstruction⁴⁵ could also potentially speed up acquisition.

The enhanced signal from blood vessels in the subtraction images allowed visualization of the entire thoracic vasculature at least until the segmental arteries, without requiring contrast agent injection. This could not easily be offered with a turbo-spin echo acquisition, as obtaining a bright-blood image with the same contrast properties is not possible. Inversion recovery methods⁴⁶ could allow similar image subtraction but the coverage of a complete 3D volume requires complicated planning of the acquisition to ensure proper inflow of inverted blood.²⁶ Time of flight methods could also be potentially used but their lower spatial resolution as well as sensitivity to susceptibility artifacts⁴⁷ and multiplanar flow directionality⁴⁸ may limit their use for lung imaging.

Improved diaphragm definition was only seen in the expiratory datasets (frame 1 and 2), as the amplitude of

respiratory motion in healthy volunteers is narrower in that range than in the inspiratory range.⁸ Further studies are required to evaluate the efficiency of this algorithm in patients with lung disease who may have different breathing patterns.³⁴

Finally, this technique has been successfully applied in 2 CF patients. In the context of lung disease, this sequence may help to better identify mucoid plugging even if the boundary between vessel and airway cannot be directly visualized due to the small size of these structures. Side-by-side comparison of subtraction images with the black-blood images can help confirm the presence of mucoid impactions within bronchi of variable caliber. Indeed, the disappearance of these structures on subtraction images confirms the nonvascular or stationary source of the signal. In addition, the residual signal of some arteries in black-blood images should present as thinner than normal arteries due to physiological vasoconstriction secondary to hypoventilation. Therefore, confusion with abnormal airways as those encountered in CF appears less probable.

In addition to the differences in flow velocity between blood and mucoid impaction, the differences² in T_2 may also contribute additionally to signal enhancement. This may be of value to further characterize the content of mucoid impactions.⁴⁹ A limitation of the studied technique is that in the absence of contrast agent injection, differentiating bronchial wall thickening from mucoid impactions is not possible. However, the value of avoiding contrast agent injection needs to be taken into account,⁵⁰ especially for patients requiring multiple follow-up studies. Further studies are required to fully assess the benefits in patients of the new proposed sequence taking into account these limitations.

Subtraction images may also allow an assessment of the vasculature in these patients, particularly the detection of hypertrophied systemic bronchial and nonbronchial arteries, which may have a clinical value in the management of patients. The good visualization of proximal pulmonary arteries could also potentially be of use to rule out central pulmonary embolism⁵¹ in case of unexplained gazometric deterioration.

The disappearance of signal from mucoid plugging in maximum intensity projections of subtraction images confirmed the good overlap between the 2 datasets, as misregistration would result in artifacts, such as imperfect signal suppression and doubling of structures in the images. The patient subtraction dataset displayed similar image quality to the one seen in healthy volunteers. Whether this good image quality can be reliably achieved in a majority of patients remains to be investigated in further studies, as irregular breathing patterns could potentially have a detrimental effect on proper alignment of images. As only a single patient subtraction dataset was available, artery visibility remains to be quantified in a subsequent patient study.

In conclusion, we preliminarily demonstrated the technical feasibility of a new method that may facilitate the detection of mucoid impactions in CF patients while

allowing an assessment of vasculature without contrast agent injection. While the free-breathing acquisition also may contribute to greater tolerance of the procedure, the exact clinical value remains to be investigated in dedicated patient studies.

ACKNOWLEDGMENT

The authors thank David Rotzinger for his help.

ORCID

Jean Delacoste  <https://orcid.org/0000-0002-9936-2698>

Giulia Ginami  <https://orcid.org/0000-0003-4669-0572>

Ruud B. van Heeswijk  <https://orcid.org/0000-0001-5028-4521>

REFERENCES

- Biederer J, Beer M, Hirsch W, et al. MRI of the lung (2/3). Why ... when ... how? *Insights Imaging*. 2012;3:355–371.
- Puderbach M, Eichinger M. The role of advanced imaging techniques in cystic fibrosis follow-up: is there a place for MRI? *Pediatr Radiol*. 2010;40:844–849.
- Stahl M, Wielpütz MO, Graeber SY, et al. Comparison of lung clearance index and magnetic resonance imaging for assessment of lung disease in children with cystic fibrosis. *Am J Respir Crit Care Med*. 2017;195:349–359.
- Wild J, Marshall H, Bock M, et al. MRI of the lung (1/3): methods. *Insights Imaging*. 2012;3:345–353.
- Bergin CJ, Pauly JM, Macovski A. Lung parenchyma: projection reconstruction MR imaging. *Radiology*. 1991;179:777–781.
- Nielles-Vallespin S, Weber M-A, Bock M, et al. 3D radial projection technique with ultrashort echo times for sodium MRI: clinical applications in human brain and skeletal muscle. *Magn Reson Med*. 2007;57:74–81.
- Dournes G, Menut F, Macey J, et al. Lung morphology assessment of cystic fibrosis using MRI with ultra-short echo time at submillimeter spatial resolution. *Eur Radiol*. 2016;26:3811–3820.
- Delacoste J, Chaptinel J, Beigelman C, Piccini D, Sauty A, Stuber M. A double echo ultra-short echo time (UTE) acquisition for respiratory motion suppressed high resolution imaging of the lung. *Magn Reson Med*. 2018;79:2297–2305.
- Nagle SK, Francois CJ, Poranski ME, Bell LC, Johnson KM, Fain SB. 3D radial UTE MRI outperforms 3D cartesian conventional echo time MRI for evaluation of cystic fibrosis lung disease. In: Proceedings of the 25th Annual Meeting of ISMRM, Honolulu, Hawaii, 2017. Abstract 0833.
- Delacoste J, Beigelman C, Feng L, et al. Assessment of cystic fibrosis disease using UTE imaging with XD-GRASP reconstruction: a comparison with CT. In: Proceedings of the 25th Annual Meeting of the ISMRM, Honolulu, HI, 2017. Abstract 0829.
- Bhalla M, Turcios N, Aponte V, et al. Cystic fibrosis: scoring system with thin-section CT. *Radiology*. 1991;179:783–788.
- Wielpütz M, Kauczor H-U. MRI of the lung – state of the art. *Diagn Interv Radiol*. 2012;18:344–353.
- Eichinger M, Heussel C-P, Kauczor H-U, Tiddens H, Puderbach M. Computed tomography and magnetic resonance imaging in cystic fibrosis lung disease. *J Magn Reson Imaging*. 2010;32:1370–1378.
- Edelman RR, Chien D, Kim D. Fast selective black blood MR imaging. *Radiology*. 1991;181:655–660.
- Simonetti OP, Finn JP, White RD, Laub G, Henry DA. “Black blood” T2-weighted inversion-recovery MR imaging of the heart. *Radiology*. 1996;199:49–57.
- Brinson GM, Noone PG, Mauro MA, et al. Bronchial artery embolization for the treatment of hemoptysis in patients with cystic fibrosis. *Am J Respir Crit Care Med*. 1998;157:1951–1958.
- Yoon W, Kim JK, Kim YH, Chung TW, Kang HK. Bronchial and nonbronchial systemic artery embolization for life-threatening hemoptysis: a comprehensive review. *Radiographics*. 2002;22:1395–1409.
- Chung MJ, Lee JH, Lee KS, Yoon YC, Kwon OJ, Kim TS. Bronchial and nonbronchial systemic arteries in patients with hemoptysis: depiction on MDCT angiography. *AJR Am J Roentgenol*. 2006;186:649–655.
- Mundo-Sagardia JA, Januzzi JL, Cury RC. Hypertrophied bronchial artery in cystic fibrosis diagnosed by computed tomography angiography. *J Cardiovasc Comput Tomogr*. 2007;1:110–111.
- Wielpütz MO, Eichinger M, Puderbach M. Magnetic resonance imaging of cystic fibrosis lung disease. *J Thorac Imaging*. 2013;28:151–159.
- Okada Y, Ohtomo K, Kiryu S, Sasaki Y. Breath-hold T2-weighted MRI of hepatic tumors: value of echo planar imaging with diffusion-sensitizing gradient. *J Comput Assist Tomogr*. 1998;22:364–371.
- Delacoste J, Feliciano H, Ginami G, van Heeswijk RB, Piccini D, Stuber M. Black-blood ultra short echo time (UTE) imaging of the thoracic vessels. In: Proceedings of the 28th International Conference of Society for Magnetic Resonance Angiography, Chicago, Illinois, 2016.
- Fan Z, Sheehan J, Bi X, Liu X, Carr J, Li D. 3D noncontrast MR angiography of the distal lower extremities using flow-sensitive dephasing (FSD)-prepared balanced SSFP. *Magn Reson Med*. 2009;62:1523–1532.
- Nielsen HT, Gold GE, Olcott EW, Pauly JM, Nishimura DG. Ultra-short echo-time 2D time-of-flight MR angiography using a half-pulse excitation. *Magn Reson Med*. 1999;41:591–599.
- O’Brien KR, Myerson SG, Cowan BR, Young AA, Robson MD. Phase contrast ultrashort TE: a more reliable technique for measurement of high-velocity turbulent stenotic jets. *Magn Reson Med*. 2009;62:626–636.
- Koktzoglou I, Li D. Diffusion-prepared segmented steady-state free precession: application to 3D black-blood cardiovascular magnetic resonance of the thoracic aorta and carotid artery walls. *J Cardiovasc Magn Reson*. 2007;9:33–42.
- Piccini D, Littmann A, Nielles-Vallespin S, Zenge MO. Spiral phyllotaxis: the natural way to construct a 3D radial trajectory in MRI. *Magn Reson Med*. 2011;66:1049–1056.
- Piccini D, Littmann A, Nielles-Vallespin S, Zenge MO. Respiratory self-navigation for whole-heart bright-blood coronary MRI: methods for robust isolation and automatic segmentation of the blood pool. *Magn Reson Med*. 2012;68:571–579.
- van Heeswijk RB, Feliciano H, Bongard C, et al. Free-breathing 3 T magnetic resonance T2-mapping of the heart. *JACC: Cardiovasc Imaging*. 2012;5:1231–1239.

30. Haase A. Snapshot flash MRI applications to T1, T2, and chemical-shift imaging. *Magn Reson Med.* 1990;13:77–89.
31. Brittain JH, Hu BS, Wright GA, Meyer CH, Macovski A, Nishimura DG. Coronary angiography with magnetization-prepared T2 contrast. *Magn Reson Med.* 1995;33:689–696.
32. Nezafat R, Stuber M, Ouwerkerk R, Gharib AM, Desai MY, Pettigrew RI. B1-insensitive T2 preparation for improved coronary magnetic resonance angiography at 3T. *Magn Reson Med.* 2006;55:858–864.
33. Nguyen TD, de Rochefort L, Spincemaille P, et al. Effective motion-sensitizing magnetization preparation for black blood magnetic resonance imaging of the heart. *J Magn Reson Imaging.* 2008;28:1092–1100.
34. Ginami G, Bonanno G, Schwitter J, Stuber M, Piccini D. An iterative approach to respiratory self-navigated whole-heart coronary MRA significantly improves image quality in a preliminary patient study. *Magn Reson Med.* 2016;75:1594–1604.
35. Piccini D, Feng L, Bonanno G, et al. Four-dimensional respiratory motion-resolved whole heart coronary MR angiography. *Magn Reson Med.* 2016;77:1473–1484.
36. Feng L, Axel L, Chandarana H, Block KT, Sodickson DK, Otazo R. XD-GRASP: golden-angle radial MRI with reconstruction of extra motion-state dimensions using compressed sensing. *Magn Reson Med.* 2016;75:775–788.
37. Yerly J, Ginami G, Nordio G, et al. Coronary endothelial function assessment using self-gated cardiac cine MRI and k-t sparse SENSE. *Magn Reson Med.* 2015;76:1443–1454.
38. Pipe JG. Motion correction with PROPELLER MRI: application to head motion and free-breathing cardiac imaging. *Magn Reson Med.* 1999;42:963–969.
39. Ciet P, Serra G, Bertolo S, et al. Assessment of CF lung disease using motion corrected PROPELLER MRI: a comparison with CT. *Eur Radiol.* 2016;26:780–787.
40. Meier-Schroers M, Kukuk G, Homsy R, Skowasch D, Schild HH, Thomas D. MRI of the lung using the PROPELLER technique: artifact reduction, better image quality and improved nodule detection. *Eur J Radiol.* 2016;85:707–713.
41. Holm S. A simple sequentially rejective multiple test procedure. *Scand J Stat.* 1979;6:65–70.
42. Tibiletti M, Paul J, Bianchi A, et al. Multistage three-dimensional UTE lung imaging by image-based self-gating. *Magn Reson Med.* 2016;75:1324–1332.
43. Dixon WT. Simple proton spectroscopic imaging. *Radiology.* 1984;153:189–194.
44. Ridgway JP. Cardiovascular magnetic resonance physics for clinicians. *Part I: J Cardiovasc Magn Reson.* 2010;12:71.
45. Doneva M, Börnert P, Eggers H, Stehning C, SÉNÉgas J, Mertins A. Compressed sensing reconstruction for magnetic resonance parameter mapping. *Magn Reson Med.* 2010;64:1114–1120.
46. Mai VM, Chen Q, Bankier AA, et al. Imaging pulmonary blood flow and perfusion using phase-sensitive selective inversion recovery. *Magn Reson Med.* 2000;43:793–795.
47. van Beek EJ, Wild JM, Fink C, Moody AR, Kauczor H-U, Oudkerk M. MRI for the diagnosis of pulmonary embolism. *J Magn Reson Imaging.* 2003;18:627–640.
48. Johns CS, Swift AJ, Hughes PJ, Ohno Y, Schiebler M, Wild JM. Pulmonary MR angiography and perfusion imaging—a review of methods and applications. *Eur J Radiol.* 2017;86:361–370.
49. Dournes G, Berger P, Refait J, et al. Allergic bronchopulmonary aspergillosis in cystic fibrosis: MR imaging of airway mucus contrasts as a tool for diagnosis. *Radiology.* 2017;285:261–269.
50. Branch SM, Tweedle MF, Orton CG. The use of gadolinium-based contrast agents should be discontinued until proven safe. *Med Phys.* 2017;44:3371–3374.
51. Takemoto CM. Venous thromboembolism in cystic fibrosis. *Pediatr Pulmonol.* 2011;47:105–112.

How to cite this article: Delacoste J, Feliciano H, Yerly J, et al. A black-blood ultra-short echo time (UTE) sequence for 3D isotropic resolution imaging of the lungs. *Magn Reson Med.* 2019;81:3808–3818. <https://doi.org/10.1002/mrm.27679>